Published by
NIGERIAN SOCIETY OF PHYSICAL SCIENCES
Available online @ https://journal.nsps.org.ng/index.php/jnsps

J. Nig. Soc. Phys. Sci. 7 (2025) 2696

Journal of the Nigerian Society of Physical Sciences

# Response of the magnetospheric convection electric field (MCEF) to geomagnetic storms during the solar cycle 24 declining phase

Nongobsom Bazié[a], Christian Zoundi[a,*], M'BI Kaboré[b], Alfred Jean Stéphane Dama[a], Frédéric Ouattara[a]

[a]*Laboratoire de Chimie Analytique, de Physique Spatiale et Énergétique (L@CAPSE), Université Norbert ZONGO, Koudougou, Burkina Faso*
[b]*Laboratoire de Matériaux, d'Héliophysique et Environnement (La.M.H.E), ED/ST, Université Nazi BONI, 01 BP 1091, Bobo-Dioulasso, Burkina Faso*

## Abstract

This article examines the magnetospheric convection electric field (MCEF) fluctuations during seven moderate to severe storms in the declining phase of solar cycle 24. The storms induced by ICMEs were selected based on specific conditions. The primary aim of this study is to assess the influence of geoeffective ICMEs on the MCEF. We conducted a cross-correlation analysis to examine the temporal delays between MCEF fluctuations and geomagnetic indices (Sym-H and AE), as well as the IMF Bz. A linear regression was employed to assess MCEF fluctuations in relation to variations in Sym-H, AE, and Bz. A strong correlation ($R$ = 0.81) was seen between the average transit speed of ICMEs and MCEF fluctuations in the initial phase, underscoring the direct influence of ICMEs on the MCEF. ICMEs with speeds ≥ 800 km/s cause substantial MCEF variations during the storm's initial phase, with a variation of 0.08 mV/m for every one nT change in IMF Bz. During the complete evolution of the examined storms, fluctuations in the AE index precede those of the MCEF, with time delays between 21 and 44 minutes. MCEF variations exhibit a delay relative to Sym-H index fluctuations, with estimated intervals ranging from 60 to 306 minutes.

DOI:10.46481/jnsps.2025.2696

*Keywords:* Geomagnetic storm, Geoeffective interplanetary coronal mass ejections, Magnetospheric convection electric field, Solar cycle

*Article History :*
Received: 26 February 2025
Received in revised form: 12 May 2025
Accepted for publication: 09 June 2025
Published: 13 August 2025



Communicated by: B. J. Falaye

## 1. Introduction

The Sun is a plasma sphere that interacts with geospace via solar radiation and wind under the influence of its magnetic field. During this interaction, the solar wind (SW) transfers an enormous amount of energy and matter to Earth's environment through coronal mass ejections (CMEs) and corotating interaction regions (CIRs) [1–5]. The energy transferred to Earth's environment then influences the geomagnetic field [6–8].

A geomagnetic storm (GMS) occurs when the flow of matter and energy from the solar wind into the magnetosphere is intense and prolonged [9]. The widely used geomagnetic indices to measure the various geomagnetic disturbances during GMSs are the Dst (Disturbance Storm Time) index and the AE (Auroral Electrojet) index [10, 11]. The Dst index represents the decrease in the average longitudinal geomagnetic

*Corresponding author: Tel.: 002-267-144-4242
*Email address:* zounchr@yahoo.fr (Christian Zoundi)

field at low latitudes, which is the most common approach for detecting the strength of GMSs and the magnetospheric ring current [7, 12, 13]. On the other hand, the AE index quantifies the overall activity of the auroral electrojet in the auroral zone [14]. Currently, the Sym-H (Symmetric Horizontal) index is used for greater accuracy in describing the strength of GMSs [15–17]. Nowadays, the impact of GMSs on human activities has led to growing interest in their prediction. Current approaches generally fall into three main categories: physical models [18, 19], statistical models [20] and machine learning methods. Machine learning methods have recently emerged as powerful tools for capturing complex nonlinear relationships within high-dimensional datasets [21–23].

GMSs are classified according to the Dst index as follows : (1) Weak ($-50$ nT < Dst ≤ $-30$ nT), (2) Moderate ($-100$ nT < Dst ≤ $-50$ nT), (3) Intense (-200 nT < Dst ≤ $-100$ nT), (4) Severe ($-350$ nT < Dst ≤ $-200$ nT), and (5) Extreme (Dst ≤ $-350$ nT) [24, 25]. Intense and severe GMSs are typically induced by solar phenomena such as inter planetary coronal mass ejections (ICMEs) [26–30].

The SW carries a portion of the Sun's magnetic field with it. The solar magnetic field carried by the SW is called the interplanetary magnetic field (IMF) Bz. Combining the IMF Bz component and the SW with velocity Vx generates an interplanetary electric field (IEF) Ey. Additionally, the coupling between the SW and Earth's magnetosphere creates, through a dynamo effect, an electric field called the magnetospheric electric field, which is oriented from dawn to dusk and induces plasma motion (or convection) from the magnetotail toward Earth[31–33].

Numerous studies have been conducted on magnetospheric dynamics, particularly on the injection and acceleration of particles within the magnetosphere, as well as the convection of low-energy magnetospheric plasma, by various researchers [34–42]. Magnetic reconnection, as described by Dungey [34, 35], is now well recognised as the principal mechanism for the transfer of energy, matter, and momentum from the SW to the magnetosphere. The MCEF is influenced by geomagnetic activity [36, 37, 40], the orientation of the IMF Bz [39, 41, 42] and the IEF Ey [38]. Figure 1 illustrates the two magnetic reconnection configurations based on the Dungey model, which helps explain specific responses of the MCEF depending on the orientation of the IMF Bz.

Lei *et al.* [38] established a robust empirical linear relationship between the MCEF and the IEF Ey. This relationship was validated by Revah and Beauer [43]. Nevertheless, the formula proposed by Lei *et al.* [38] has rarely been employed in research concerning magnetospheric convection. Before this study, other investigations, including those by Rostoker [11], Smart *et al.* [44], and Baker *et al.* [45], and Meloni *et al.* [46] had already analysed the cross-correlation between the IEF Ey and the AE and Dst indices during GMSs. Nishimura *et al.* [47] directly used Ey as an estimate of the MCEF. Rostoker [48] and Baker *et al.* [45] used high temporal resolution data (5 minutes and 2.5 minutes, respectively), while Smart *et al.* [44] and Meloni *et al.* [46] relied on data with hourly resolution. Nishimura *et al.* [47] demonstrated an almost immediate response of Ey to variations in Bz with a one-minute temporal resolution, although they did not explore a quantitative relationship.

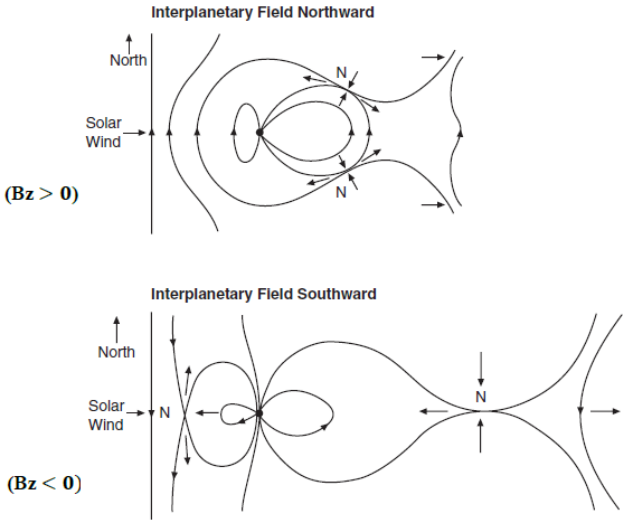


Figure 1. Dungey's two models of the reconnecting magnetosphere. The top panel shows the case of an IMF Bz northward , and the bottom panel shows an IMF Bz southward. The points labelled 'N' are neutral points or reconnection sites. The horizontal arrows show the direction of accelerated plasma flows. (source: Bothmer *et al.* [39]).

Recently, the empirical formula proposed by Lei *et al.* [38] has been employed by Salfo and Fédéric [40], Inza *et al.* [49, 50], Salfo *et al.* [51], Stéphane *et al.* [52] and Bazié *et al.* [53]. However, these studies have primarily focused on analysing the magnetospheric convection electric field (MCEF) under geomagnetic activity conditions classified according to the four categories defined by Legrand and Simon [54] and Zerbo *et al.* [55] without emphasising specific events such as GMSs, as was the case in earlier studies.

This study analyses the MCEF's response to GMSs during the declining phase of solar cycle 24, specifically those triggered by ICMEs, using the formulation proposed by Lei *et al.* [38]. Its objective is to improve our understanding of MCEF fluctuations during geoeffective ICMEs. Weak GMSs, which have little or no significant effect on the magnetosphere, are excluded from the analysis. Thus, only moderate and intense GMSs are considered under specific conditions detailed in the methodology section. A total of seven GMSs, selected according to these particular conditions, were examined. The inclusion of moderate GMSs in this study is justified because, during these events, the Kp (planetary K) index exhibited behaviour similar to that observed during intense or severe GMSs. Finally, we focus on the temporal fluctuations of SW parameters (speed: VSW, plasma pressure: PSW, IMF Bz) and geomagnetic indices (AE, Sym-H). This analysis will provide a better understanding of the dependence between the MCEF and indices (AE, Sym-H) and SW parameters during the complete evolution of the analysed storms. We use a high resolution (1 minute) to compare the time shifts between the MCEF and the predictor indices of GMSs, such as AE, Sym-H, and Bz, with the results previously obtained. Section 2 presents the data and methods used in the study. Sections 3 and 4 report the results

and discussions. Finally, Section 5 addresses the conclusion.

## 2. Analysis methods

We analyse the response of the MCEF to Sudden Storm Commencement (SSC) GMSs. To ensure the geoeffectiveness of the associated ICME, we use the Kp and Dst indices as selection criteria. The day of the SSC is considered the first day of the storm. We focus on events where the Kp index reaches at least 6 ($Kp \geq 6$) on the SSC day or the following day and where the minimum Dst index is less than or equal to −50 nT (Dst $\leq -50$ nT). To select temporally isolated ICMEs, we identify periods of quiet magnetic conditions before and after the SSC day. A quiet day is defined by a Kp index below 3 ($Kp < 3$). This method for selecting isolated ICMEs is inspired by Azzouzi [56]. The main characteristics of the identified storms are summarised in Table 1. MCEF values were estimated using the empirical relation MCEF = 0.13Ey + 0.09, following Lei et al. [38].To examine the variability of the MCEF, we overlay the daily profiles of SW parameters (VSW, PSW, Bz), indices (Sym-H and AE), and the MCEF itself. We analyse its temporal variations by comparing them to those of the SW parameters and indices (AE, Sym-H) during the evolution of the storms. For the MCEF, the variability of the quietest day of the month is used as a reference. We will then perform a cross-correlation analysis to determine the time lags between the MCEF and the parameters (Bz, AE, Sym-H) for each storm. A linear regression analysis is conducted at the lag corresponding to the maximum correlation for each storm to assess the variations of the MCEF and the parameters (Bz, AE, Sym-H). To establish a link between the ICME and the MCEF fluctuations observed during the storm, we analyse the dependence between the average transit speeds of ICMEs (VICME), reported in Table 1, and the extreme values of the MCEF observed during the storms' initial phase. We also examine the relationship between the average transit speed of the ICME and the maximum VSW during this phase through a linear correlation analysis.

The analysis methods presented in Section 2 are inspired by those described in our previously published work (Nongobsom *et al.* [57]), where a similar approach was employed. They have, however, been slightly modified to suit the specific objectives of the present study.

## 3. Results

Figures 2 to 8 illustrate the temporal variations of VSW, PSW, Bz, Sym-H, AE, and the MCEF during the storms that occurred on 17 March 2015, 23 June 2015, 16 August 2015, 20 September 2015, 20 December 2015, 1 January 2016, and 28 May 2017. From top to bottom, the panels in each figure show the daily evolution of Bz, VSW, PSW, Sym-H, AE, and the MCEF, respectively. In the lower panel, the black graph represents the variation of the MCEF during the storm, while the blue graph corresponds to the MCEF variation on a very quiet day. The beginning of the storm is defined as the time origin ($t = 0$), marked by the first red vertical line on each figure. The space between the first and second red vertical lines corresponds to the initial phase of the storm, denoted as "I" in the figure. Similarly, the main phase, denoted as "M", is delimited by the second and third red vertical lines. Finally, the recovery phase, denoted as "R", is delimited by the third and fourth red vertical lines.

Figure 9 shows the comparative evolution of the MCEF during the analysed GMSs. The time origin ($t = 0$ *s*) corresponds to the onset of each storm. The black curve represents the evolution of the MCEF during the 17 March 2015 storm, the blue curve corresponds to the 23 June 2015 storm, and the green curve reflects its behaviour during the 16 August 2015 storm. The yellow curve indicates the MCEF evolution during the 20 September 2015 event, the orange one corresponds to the 20 December 2015 storm, the red curve represents the 1 January 2016 storm, and the violet curve represents the 28 May 2017 event.

Figure 10 presents the cross-correlation and linear regression between the MCEF and the parameters (Bz, AE, Sym-H) during the complete evolution of the storm on 17 March 2015. Panels (a), (b), and (c) show the cross-correlation between the MCEF and AE, the MCEF and Sym-H, and the MCEF and Bz, respectively. Panels (d), (e), and (f) illustrate the corresponding linear regressions. The results of the cross-correlation and linear regression applied to all the analysed storms are presented in Table 2. Figure 10 analyses, on the one hand, the relationship between the average transit speed of the ICME (VICME) and the extreme value of the MCEF observed during the initial phase and, on the other hand, the relationship between the average transit speed of the ICME and the maximum solar wind speed (VSW) during this same phase.

### 3.1. Temporal fluctuations of the MCEF during the analysed storms

In all Figures 2 to 8, we observe a convergence between the two MCEF graphs during the pre- and post-storm periods. A marked difference is observed during the different phases of the storm: the MCEF during the disturbed period is clearly above that of the very quiet period. It increases during the initial phase, amplifies further in the primary phase, and gradually decreases during recovery. By examining each storm individually, we arrive at the following quantitative analysis, taking into account the different phases of the storm:

In the initial phase, during the storm of 17 March 2015 (Figure 2), the MCEF reached a maximum of 1.74 mV/m to the west approximately 41 minutes after the start of the storm. This change is associated with a northward Bz orientation of 21 nT. A rise in Sym-H to 69 nT was observed 5 minutes before this MCEF variation. AE reached 790 nT 123 minutes after the MCEF change. Additionally, an increase in VSW of 524 km/s and PSW of 19.08 nPa was recorded 20 minutes before this change. During the storm of 23 June 2015 (Figure 3), the MCEF reached 3.29 mV/m in 21 minutes. Simultaneously, Bz oriented southward by 33 nT. At the start of the storm, Sym-H recorded a peak of 83 nT. 21 minutes later, an AE peak of 2200 nT was observed. VSW and PSW reached 712 km/s and 57 nPa, respectively. In the storm of 16 August 2015 (Figure 4),

Table 1. Characteristics of selected GMSs.

| GMS Date | SSC Date and Time | Dst (nT) | Kp | CME Issue Date and Time | Avg. ICME Speed (km/s) |
|---|---|---|---|---|---|
| 17-03-2015 | 17-03-2015 (04:45:00) | -234 | 8 | 15-03-2015 (01:48:05) | 840 |
| 23-06-2015 | 22-06-2015 (05:44:24) | -198 | 8 | 21-06-2015 (02:36:05) | 1040 |
| 16-08-2015 | 15-08-2015 (08:29:00) | -98 | 6 | 12-08-2015 (14:48:05) | 640 |
| 20-09-2015 | 20-09-2015 (06:04:00) | -81 | 7 | 18-09-2015 (05:00:06) | 850 |
| 20-12-2015 | 19-12-2015 (16:16:12) | -166 | 7 | 16-12-2015 (09:36:04) | 540 |
| 01-01-2016 | 31-12-2015 (00:49:36) | -116 | 6 | 28-12-2015 (12:12:05) | 690 |
| 28-05-2017 | 27-05-2017 (15:34:00) | -125 | 7 | 23-05-2017 (05:00:06) | 400 |

the MCEF showed a maximum of 1.25 mV/m to the east after 100 minutes. Bz exhibited a southward polarity of 17 nT during this time, while Sym-H reached 53 nT. AE recorded a peak of 1110 nT 130 minutes later. VSW and PSW reached 499 km/s and 13 nPa after 100 minutes.

During the storm of 20 September 2015 (Figure 5), the MCEF reached 1.31 mV/m after 17 minutes, Bz oriented southward by 17 nT, and AE rose to 840 nT. At the time of the shock, Sym-H increased to 8 nT. VSW reached 591 km/s, and PSW reached eight nPa. During the storm of 20 December 2015 (Figure 6), the MCEF evolved westward, reaching 0.94 mV/m after 680 minutes. At the same time, Bz exhibited a southward polarity of 18 nT. AE recorded a peak of 880 nT after 310 minutes, while Sym-H reached its peak of 46 nT after 130 minutes. VSW rose to 500 km/s after 200 minutes, and PSW reached 22 nPa after 110 minutes. In the storm of 1 January 2016 (Figure 7), the MCEF varied eastward, reaching 0.90 mV/m after 648 minutes, while Bz moved southward by 13 nT. AE peaked at 970 nT after 460 minutes, and Sym-H reached its maximum of 31 nT after 7 minutes. The maxima of VSW and PSW were 511 km/s after 310 minutes and 14 nPa after 640 minutes, respectively. Finally, during the storm of 28 May 2017 (Figure 8), the MCEF showed a change of 0.95 mV/m after 370 minutes, while Bz moved southward by 18 nT. AE recorded a peak of 570 nT at 410 minutes, while Sym-H reached 60 nT at 350 minutes. VSW peaked at 391 km/s at 250 minutes and PSW at 25 nPa at 320 minutes.

In the main phase, during the 17 March 2015 storm, the MCEF reached its maximum value of 2.11 mV/m at 480 minutes when Bz was oriented southward by 26 nT. Sym-H decreased to -234 nT at 1080 minutes, while AE peaked at 2300 nT at 550 minutes. During the 23 June 2015 storm, the MCEF peaked at 3.62 mV/m at 50 minutes in response to a southward shift of Bz by 38 nT. AE reached 2700 nT after the MCEF peak at 85 minutes, and Sym-H decreased to -208 nT at 600 minutes. During the 16 August 2015 storm, the MCEF peaked at 1.4 mV/m at 140 minutes, when Bz moved southward by 21 nT. AE peaked at 1550 nT at 170 minutes, and Sym-H decreased to -94 nT at 140 minutes. During the 20 September 2015 storm, the MCEF peaked at 1.17 mV/m at 82 minutes, while Bz was oriented southward by 14 nT. Sym-H decreased to -84 nT at 305 minutes, while the AE index peaked at 2300 nT at 73 minutes. In the 20 December 2015 storm, the MCEF peaked at 1.1 mV/m at 1770 minutes, when Bz moved southward by 17 nT. AE recorded its maximum of 1940 nT 140 minutes later, while Sym-H decreased to -165 nT at 1830 minutes. During the storm on 1 January 2016, the MCEF reached a maximum of 1.1 mV/m at 1160 minutes, while Bz moved southward by 16 nT. AE reached 2180 nT at 710 minutes, while Sym-H decreased to -117 nT at 1454 minutes. Finally, during the storm28 May 2017, the MCEF peaked at 1.14 mV/m at 502 minutes, when Bz moved southward by 20 nT. AE reached its maximum of 1970 nT at 830 minutes, and Sym-H decreased to -142 nT at 942 minutes.

In the recovery phase, the 17 March 2015 storm is characterised by alternating peaks and troughs of the MCEF, with maxima reaching 0.85 mV/m. Bz orients southward by 11 nT. Sym-H recoveries reach -75 nT, and AE peaks at 1600 nT. During the storm on 23 June 2015, the MCEF peaks reached 1.5 mV/m, while the AE index reached 1900 nT, the Sym-H index dropped to -150 nT, and Bz reached -10 nT. In the 16 August 2015 storm, the MCEF peaks rise to 0.75 mV/m, Bz presents a southward polarity of about eight nT, and the recoveries of Sym-H reach -58 nT. AE shows a maximum of 1270 nT. During the storm on 20 September 2015, the MCEF peaks do not exceed 0.6 mV/m, with Bz oriented southward by about eight nT, the recoveries of Sym-H not exceeding -40 nT, and AE reaching peaks of 1270 nT. During the storm on 20 December 2015, the MCEF peaks reach 0.7 mV/m, and Bz presents a southward polarity of 9 nT. Sym-H recoveries do not exceed -40 nT, while AE peaks at 960 nT. In the 1 January 2016 storm, the MCEF showed peaks of 0.4 mV/m, and Bz dropped to -5 nT. AE maxima reach 590 nT, and Sym-H presents a southward polarity of -40 nT. Finally, during the 28 May 2017 storm, the MCEF reached a maximum of 0.82 mV/m, and Bz reached -14 nT. The Sym-H index drops to -40 nT, while the AE index peaks at 970 nT.

### *3.2. Comparison of the evolution of the MCEF during the analysed GMSs*

Figure 9 shows that the MCEF amplitudes during the 23 June 2015 storm stand out from those recorded during other storms in the 0 to 720-minute interval. During this event, the MCEF exhibited peak values exceeding 2.5 mV/m and minima below –2 mV/m. In the case of the 17 March 2015 storm, maximum MCEF amplitudes reached approximately 2 mV/m over the same time interval. This was followed by the storms of 28 May 2017 and 20 September 2015, during which the MCEF amplitudes peaked at around 1 mV/m. Between 1140 and 2160 minutes, the MCEF associated with the 20 December 2015 and

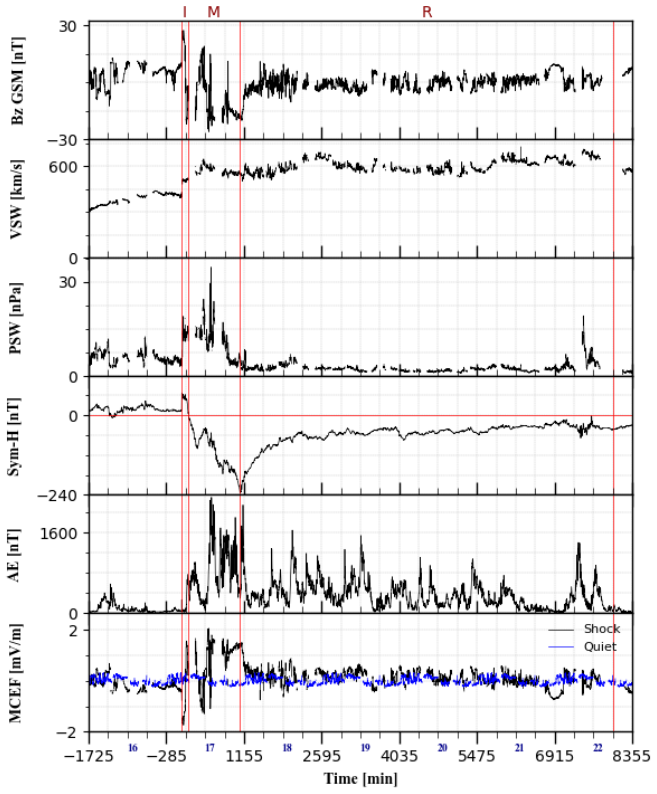


Figure 2. Daily variations of the IMF Bz, the solar wind speed (VSW), the plasma pressure (PSW), the Sym-H index, the AE index, and the MCEF from 16 March to 22 March 2015.

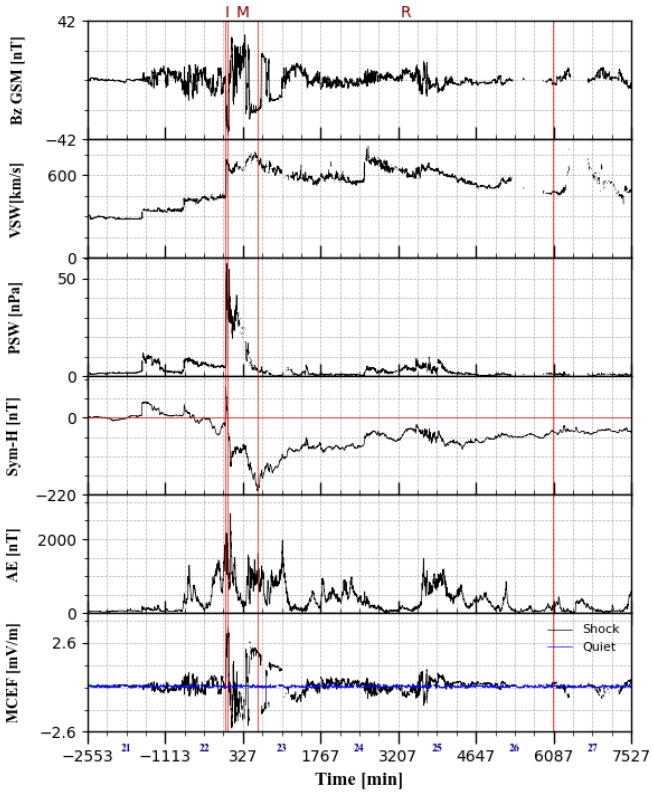


Figure 3. Daily variations of the IMF Bz, the solar wind speed (VSW), the plasma pressure (PSW), the Sym-H index, the AE index, and the MCEF from 21 June to 27 June 2015.

1 January 2016 storms also stands out, with maxima close to 1 mV/m. Overall, the MCEF amplitudes gradually decrease for all storms and tend to converge after 4320 minutes, with maximum values approaching 0.5 mV/m.

### *3.3. Cross-correlation analysis*

The analysis in Figure 10 shows that during the complete evolution of the storm on 17 March 2015, the MCEF, delayed by 21 minutes, positively correlates with the AE index (panel a), with a correlation coefficient of 0.71. It exhibits an anti-correlation with Sym-H, with a time delay of 64 minutes and an anti-correlation coefficient of -0.72 (panel b). Additionally, the MCEF is strongly anti-correlated, with no time delay, to Bz (panel c), with an anti-correlation coefficient of -0.99. Each one nT change in AE (panel d) is associated with a change of 0.000976 mV/m in MCEF 21 minutes later. A decrease (or increase) of 1 nT in Sym-H (panel e) is related to an increase (or decrease) of 0.00667 mV/m in MCEF 64 minutes later. Finally, any increase (or decrease) of 1 nT in Bz (panel f) is associated with a reduction (or increase) of 0.0696 mV/m in MCEF.

The results of the cross-correlation analysis applied to all the storms analysed are presented in Table 2. The time delay (in minutes) and the correlation coefficient (R) are listed. The analysis of Table 2 shows that during the complete evolution of all storms, the delayed MCEF correlates well with AE. The time delays range from 21 to 44 minutes, and the correlation coefficients range from 0.43 to 0.86. The positive correlations indicate a direct relationship between the fluctuations of MCEF and those of AE. This shows that the variations of MCEF are strongly linked to those of AE. The correlations between MCEF and Sym-H are negative for all storms, with positive time delays ranging from 60 to 306 minutes. This indicates that during the storms' complete evolution, the MCEF variations follow those of the Sym-H index. Finally, a nearly constant and robust correlation ($R \approx -1$) between MCEF and Bz is observed in all the analysed storms, with no time delay (lag = 0). This indicates an immediate relationship between MCEF and the IMF Bz.

The analysis of the linear regressions between MCEF and the AE index at different time delays informs us that each increase (or decrease) of the auroral activity index of 1 nT is associated with an increase (or decrease) in MCEF of 0.000731 mV/m 34 minutes later during the storm on 23 June 2015, 0.000576 mV/m 28 minutes later during the storm on 16 August 2015, 0.000536 mV/m 44 minutes later during the storm on 20 September 2015, 0.000884 mV/m 16 minutes later during the storm on 20 December 2015, 0.000671 mV/m 19 minutes later during the storm on 1 January 2016, and 0.000863 mV/m 34 minutes later during the storm on 28 May 2017. The analysis of linear regressions between MCEF and the Sym-H index at different time delays reveals that for each decrease (or increase) of 1 nT in the annular current index, there is a corresponding increase (or decrease) in MCEF of 0.00667 mV/m, 64 minutes later during the 17 March 2015 storm; 0.00382 mV/m,

Table 2. Time delays (lag) and cross-correlation coefficients (R) between MCEF and (AE, Sym-H, Bz) during the complete evolution of the storms in the descending phase.

*Note:* Lag refers to the time shift between the MCEF and AE, Sym-H, or Bz, for which the correlation coefficient *R* is extremal.

| GMS Date | MCEF vs AE | | MCEF vs Sym-H | | MCEF vs Bz | |
|---|---|---|---|---|---|---|
| | Lag | R | Lag | R | Lag | R |
| 17-03-2015 | 21 | 0.71 | 64 | -0.72 | 0 | -0.99 |
| 23-06-2015 | 34 | 0.43 | 60 | -0.29 | 0 | -0.99 |
| 15-07-2015 | 28 | 0.75 | 103 | -0.65 | 0 | -0.99 |
| 20-09-2015 | 44 | 0.60 | 73 | -0.40 | 0 | -0.99 |
| 20-12-2015 | 16 | 0.67 | 63 | -0.78 | 0 | -1.00 |
| 01-01-2016 | 19 | 0.71 | 108 | -0.61 | 0 | -1.00 |
| 28-05-2017 | 34 | 0.86 | 306 | -0.68 | 0 | -1.00 |

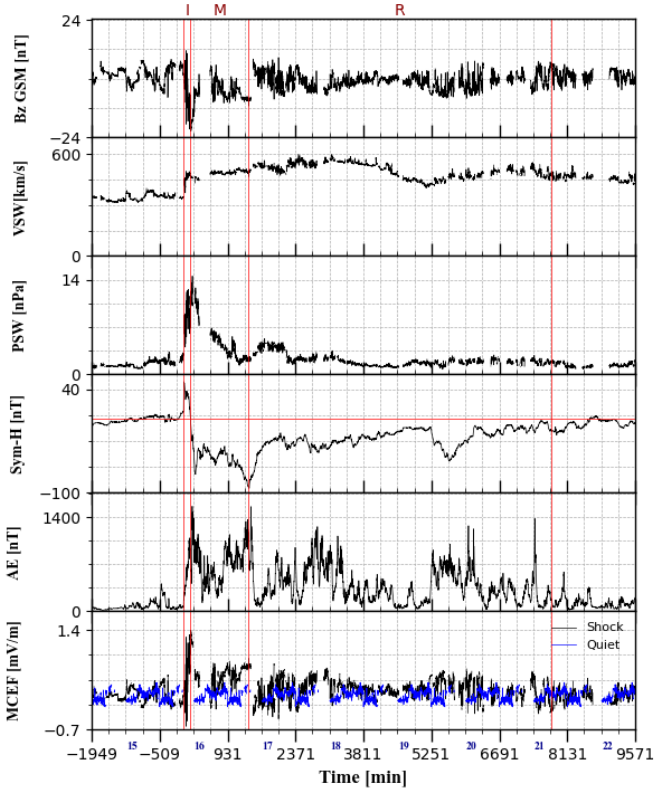


Figure 4. Daily variations of the IMF Bz, the solar wind speed (VSW), the plasma pressure (PSW), the Sym-H index, the AE index, and the MCEF from 15 August to 22 August 2015.

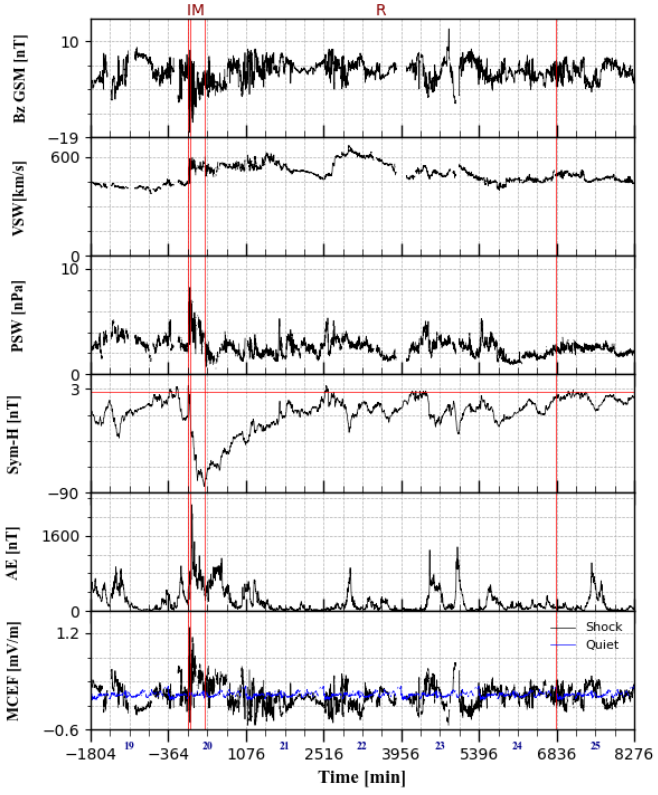


Figure 5. Daily variations of the IMF Bz, the solar wind speed (VSW), the plasma pressure (PSW), the Sym-H index, the AE index, and the MCEF from 19 September to 25 September 2015.

60 minutes later during the 23 June 2015 storm; 0.00678 mV/m, 103 minutes later during the 16 August 2015 storm; 0.00567 mV/m, 73 minutes later during the 20 September 2015 storm; 0.00598 mV/m, 63 minutes later during the 20 December 2015 storm; 0.00637 mV/m, 108 minutes later during the 1 January 2016 storm; and 0.00599 mV/m, 306 minutes later during the 28 May 2017 storm. Finally, the analysis of linear regressions between MCEF and Bz shows that every increase (or decrease) of 1 nT is associated with a reduction (or increase) of MCEF by 0.0696 mV/m during the 17 March 2015 storm; 0.0822 mV/m during the 23 June 2015 storm; 0.0603 mV/m during the 16 August 2015 storm; 0.0651 mV/m during the 20 September 2015 storm; 0.0546 mV/m during the 20 December 2015 storm; 0.058 mV/m during the 1 January 2016 storm; and 0.0481 mV/m during the 28 May 2017 storm.

### *3.4. Dependence between MCEF and ICME transit speed*

Table 3 summarises the extreme values of the MCEF recorded during the initial phase, the maximum solar wind velocities in the initial phase, and the average transit speeds of ICMEs. The direction (East or West) of the MCEF is also indicated, as it is essential for understanding the effects of the MCEF on the magnetosphere. From Table 3, it is observed that the speed of ICMEs ranges from 400 km/s (Storm of 28 May 2017) to 1040 km/s (Storm of 23 June 2015), while the solar

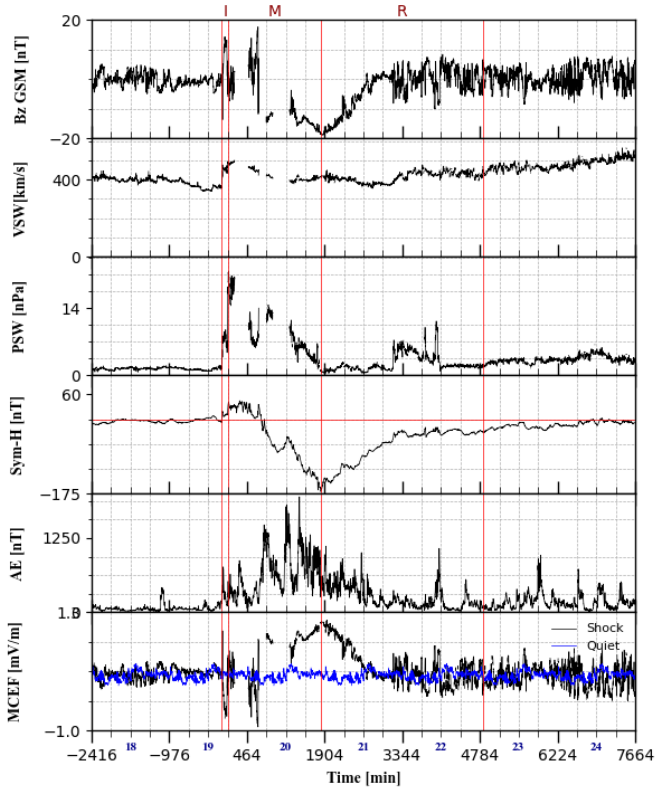


Figure 6. Daily variations of the IMF Bz, the solar wind speed (VSW), the plasma pressure (PSW), the Sym-H index, the AE index, and the MCEF from 18 December to 24 December 2015.

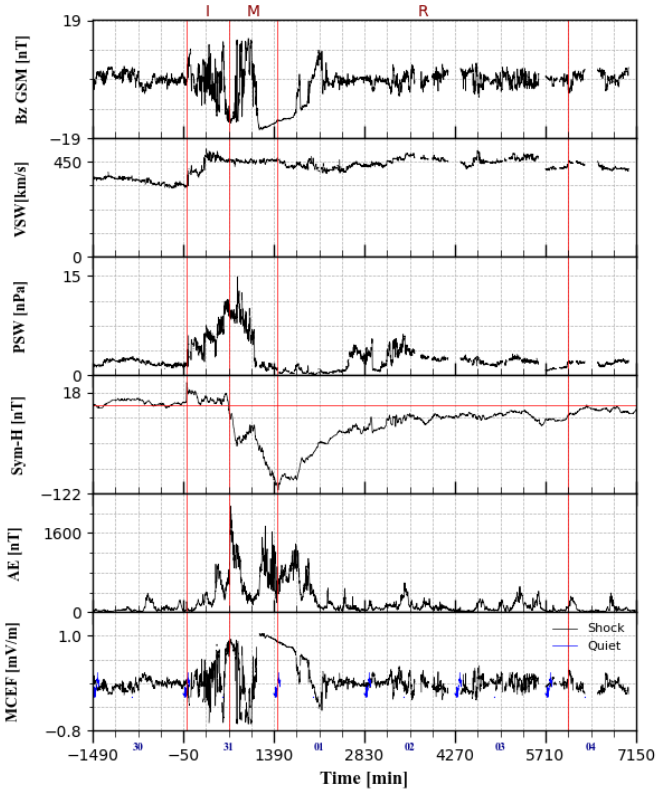


Figure 7. Daily variations of the IMF Bz, the solar wind speed (VSW), the plasma pressure (PSW), the Sym-H index, the AE index, and the MCEF from 30 December 2015 to 4 January 2016.

wind velocity fluctuates between 391 km/s (Storm of 28 May 2017) and 713 km/s (Storm of 23 June 2015). The MCEF values range from 0.90 mV/m (Storm of 1 January 2016) to 3.39 mV/m (Storm of 23 June 2015). In 71% of storms, the MCEF exhibits an Eastward orientation during the initial phase. The storms of 17 March 2015, 23 June 2015, and 20 September 2015 are associated with fast ICMEs (VICME $\geq$ 800 km/s) and intense electric fields (MCEF $\geq$ 1.31 mV/m). It could, therefore, be concluded that these storms are potentially more disruptive to the MCEF. The remaining storms, which are associated with slow ICMEs (VICME $\leq$ 690 km/s) and weak electric fields (MCEF $\leq$ 1.25 mV/m), are less disruptive to the MCEF. Finally, the moderate storms of 20 September 2015 (Dst = −81 nT and Kp = 7 nT) and 16 August 2015 (Dst = −98 nT and Kp = 6 nT) are more disruptive to the MCEF compared to the intense storms of 20 December 2015 (Dst = −166 nT and Kp = 7 nT) and 1 January 2016 (Dst = −116 nT and Kp = 6 nT). These observations indicate that the MCEF response does not depend on the magnetic disturbance level. The data for MCEF, VSW, and VICME from Table 3 were used to plot the graphs in Figure 11. Analysis of the graph in panel (a) of Figure 11 indicates a strong linear correlation between the transit speed of the ICME and the maximum solar wind speed observed in the initial phase ($R$ = 0.93). Similarly, the graph in panel (b) indicates a strong correlation between the average transit speed of the ICME and the MCEF extremum observed in the initial phase, with a correlation coefficient of $R$ = 0.81.

## 4. Discussions

Our study revealed a significant influence of the transit speed of the ICME responsible for the storm on the maximum solar wind speed observed during the initial phase of storms. Specifically, higher transit speeds of geoeffective ICMEs correspond to higher VSW values during the initial phase and vice versa. These observations align with those of Kelley *et al.* [58], Singh *et al.* [59] and Subedi *et al.* [4], which suggests that the arrival of a geoeffective ICME at the magnetosphere generates a shock wave, leading to an increase in VSW during the initial phase of the resulting storm. Furthermore, the strong correlation between the extrema of MCEF during the initial phase and the ICME transit speed likely reflects the influence of geoeffective ICMEs on MCEF fluctuations. ICMEs with transit speeds between 800 and 1040 km/s caused MCEF extrema ranging from 1.31 to 3.39 mV/m over 21 to 41 minutes. In contrast, those with velocities between 400 and 690 km/s induced MCEF extrema ranging from 0.90 to 1.25 mV/m, ranging from 70 to 680 minutes.

Nishimura *et al.* [47] and de Sequeira *et al.* [60] demonstrated that IMF Bz responds to changes in MCEF orientation, a finding also reported by Salfo and Frédéric [40], Salfo *et al.* [51] and Stéphane *et al.* [52] in their analyses of the impacts

Table 3. Extreme values of MCEF, VSW during the initial phase, and VICMEs during the peak phase of the storms.

| GMS Date | VICME (km/s) | VSW (km/s) | MCEF (mV/m) |
|---|---|---|---|
| 17-03-2015 | 840 | 524 | 1.74 (West) |
| 23-06-2015 | 1040 | 713 | 3.39 (East) |
| 16-08-2015 | 640 | 499 | 1.25 (East) |
| 20-09-2015 | 850 | 591 | 1.31 (East) |
| 20-12-2015 | 540 | 500 | 0.94 (West) |
| 01-01-2016 | 690 | 511 | 0.90 (East) |
| 28-05-2017 | 400 | 391 | 0.95 (East) |

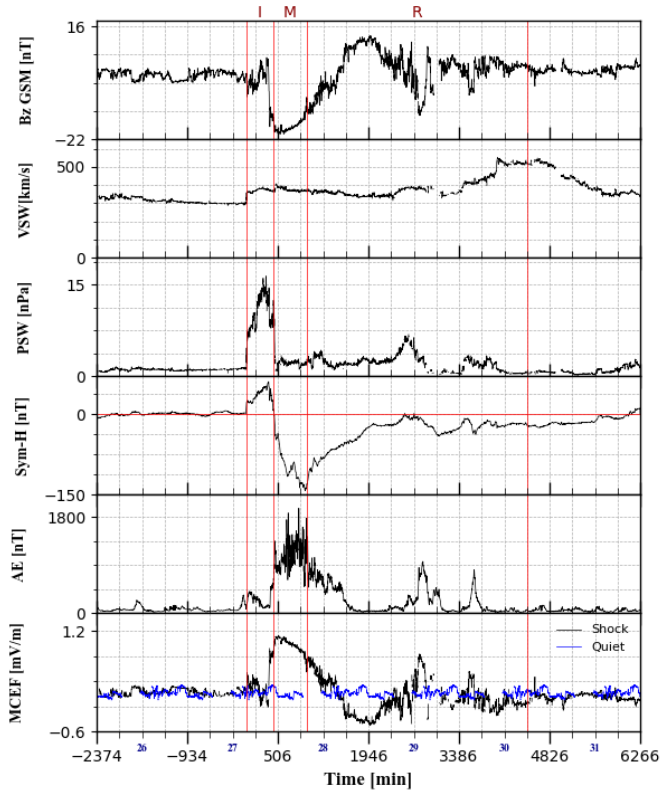


Figure 8. Daily variations of the IMF Bz, the solar wind speed (VSW), the plasma pressure (PSW), the Sym-H index, the AE index, and the MCEF from 26 May to 31 May 2017.

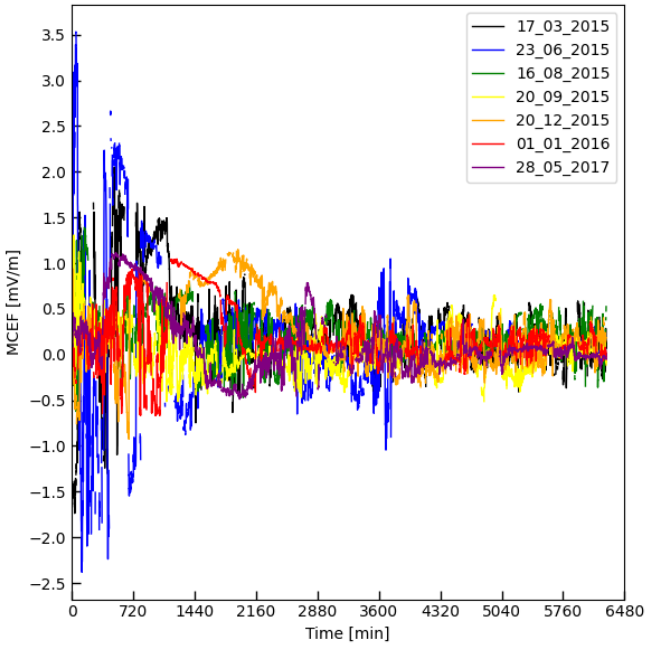


Figure 9. Comparison of the temporal profiles of MCEF during the seven analysed storms.

of geoeffective ICMEs and fast solar winds on MCEF. These results are consistent with our observations. This study extends previous work by providing minute-scale regression analyses. For example, during the declining phase storms analysed in this article, an ICME with a mean transit velocity between 400 and 690 km/s induces a Bz variation of 1 nT corresponding to an MCEF variation of approximately 0.06 mV/m. For ICMEs with speeds between 800 and 1040 km/s, a Bz variation of 1 nT results in an MCEF increase of approximately 0.08 mV/m.

MCEF fluctuations closely follow those of AE indices during storm evolution, albeit with a temporal delay. These observations corroborate the findings of Meloni *et al.* [46], who showed that the AE index correlates with the Ey, and by extension with MCEF, with a one-hour delay. However, our analysis refines this observation by examining delays on a minute scale. The linear correlation coefficients we obtained, ranging from 0.43 to 0.86, are significantly higher than those reported by Meloni *et al.* [46]. Baker *et al.* [45] reported an average delay of 40 minutes with a temporal resolution of 2.5 minutes. This average delay is significantly higher than that estimated in our study, which is 28 minutes.

The intensification of MCEF observed during the initial and main phases of storms is accompanied by an eastward or westward-oriented MCEF. An eastward-oriented MCEF corresponds to a southward-oriented Bz, a configuration favourable for magnetic reconnection [34]. Magnetic reconnection leads to a massive influx of charged particles into the magnetosphere [34, 40]. The east-west orientation of the MCEF can thus be explained by an increase in reconnection mechanisms and the accumulation of charged particles in the magnetosphere.

Studies by Salfo and Frédéric [40], Stéphane *et al.* [52] and Bazié *et al.* [53] based on statistical analyses of MCEF variability, MCEF decay phases are associated with a northward-oriented IMF Bz, indicating the absence of magnetic reconnection. However, according to Salfo and Frédéric [40], Badman

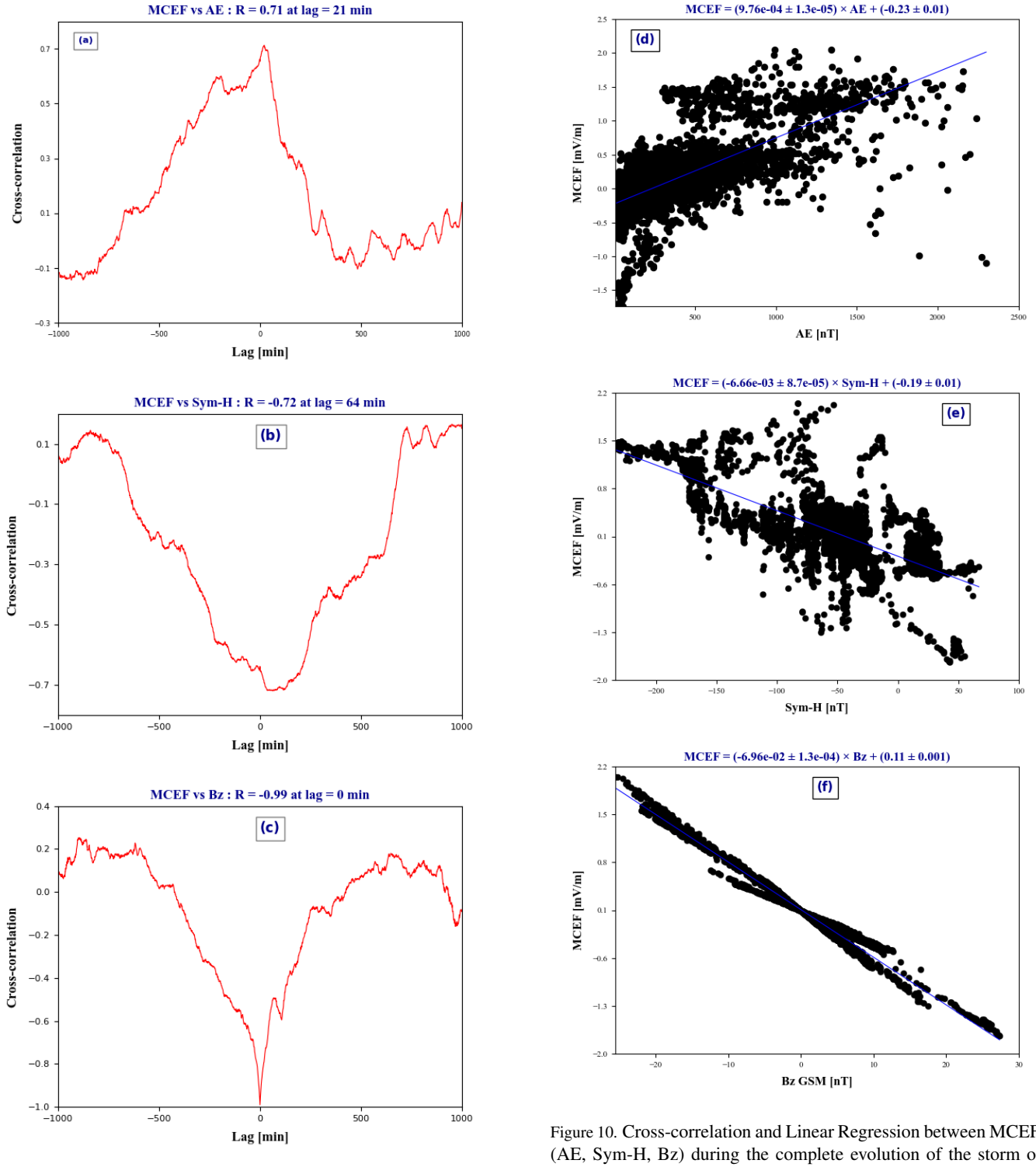


Figure 10. Cross-correlation and Linear Regression between MCEF and (AE, Sym-H, Bz) during the complete evolution of the storm on 17 March 2015.

and Cowley [61] and Siscoe *et al*. [62], magnetic reconnection can also occur with a northward-oriented IMF Bz. Our results confirm magnetic reconnection in the presence of a southward-oriented IMF Bz and support the magnetic reconnection hypothesis with a northward-oriented IMF Bz, which implies a westward-oriented MCEF. In 71% of the storms analysed, the MCEF orientation during the initial phase is eastward, suggesting that magnetic reconnection with a northward-oriented IMF Bz occurs in 29% of cases. Finally, all the GMSs analysed exhibited substorm activity during their recovery phases. The MCEF peaks preceding these substorms confirm the conclusions of Singh *et al*. [63], who indicated that the prompt

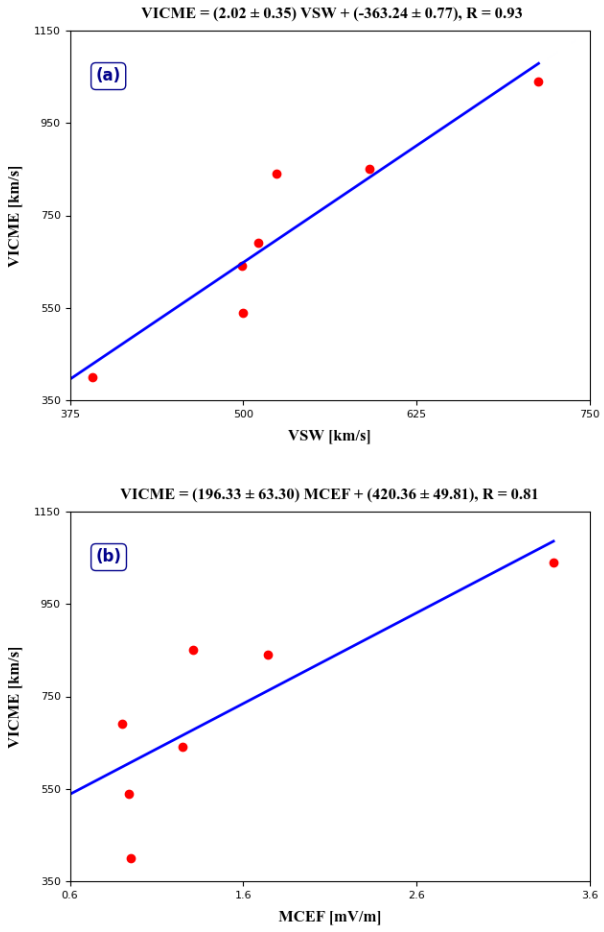


Figure 11. Correlation between VICME and a) VSW and b) MCEF variation.

penetration of the electric field induces magnetic substorms occurring during the recovery phase. Furthermore, the increase in the AE index during these substorms corroborates the findings of Lundstedt *et al.* [11] and Shadrina *et al.* [64], who identified pronounced AE peaks during the recovery phase as key indicators of magnetic substorm activity.

## 5. Conclusion

The study of MCEF variability during storms occurring in the declining phase of Solar Cycle 24 revealed a significant correlation between the average transit speed of ICMEs and MCEF variations during the initial phase, highlighting the direct impact of ICMEs on MCEF. The transit speed of ICMEs directly influences the maximum SW speed observed during the initial phase of storms. High-speed ICMEs cause pronounced MCEF variations during this phase. ICMEs with speeds between 400 and 690 km/s induce a displacement of IMF Bz by one nT, corresponding to an MCEF variation of 0.06 mV/m. Those reaching speeds between 800 and 1040 km/s generate an MCEF variation of 0.08 mV/m for every nT change of IMF Bz. During the complete evolution of the GMS, AE index variations precede those of MCEF, and MCEF variations follow those of the Sym-H index. All GMSs examined showed magnetic substorms during their recovery phases. This study contributes to the understanding of the Earth's magnetosphere dynamics. It provides information on MCEF fluctuations during GMSs, offering relevant insights to improve their forecasting.

## Data availability

The SSC dates and times, CME launch dates and times, and average ICME transit speeds presented in Table 1 are available on the following websites, respectively: https://isgi.unistra.fr/data_download.php, https://cdaw.gsfc.nasa.gov/CME_list, and https://izw1.caltech.edu/ACE/DATA/level3/icmetable2.htm. Additionally, SW parameters (VSW, PSW, Bz) are better used to assess solar activity's contribution to the magnetosphere. The Kp and Dst indices are used to characterise the identified geomagnetic storms. The AE and Sym-H indices are used to better understand their dependence on the MCEF. Minute values of the IEF Ey are used to determine the MCEF. The website, https://omniweb.gsfc.nasa.gov/form/dx1.html, provides minute values of VSW, PSW, Bz, Ey, AE, and Sym-H, as well as hourly values of Kp and Dst.

## References

[1] E. N. Parker, "Dynamics of the interplanetary gas and magnetic fields", Astrophysical Journal **128** (1958) 664. https://doi.org/10.1086/146579.
[2] B. T. Tsurutani, W. D. Gonzalez, F. Tang & Y. T. Lee, "Great magnetic storms", Geophysical Research Letters **19** (1992) 73. https://doi.org/10.1029/91GL02783.
[3] H. V. Cane, "Coronal mass ejections and Forbush decreases", Space Science Reviews **93** (2000) 55. https://doi.org/10.1023/A:1026532125747.
[4] A. Subedi, B. Adhikari & R. K. Mishra, "Variation of solar wind parameters during intense geomagnetic storms", Himalayan physics **6** (2017) 80. https://doi.org/10.3126/hj.v6i0.18366.
[5] A. Silwal, S. P. Gautam, P. Poudel, M. Karki, B. Adhikari, N. P. Chapagain, R. K. Mishra, B. D. Ghimire & Y. Migoya-Orue, "Global positioning system observations of ionospheric total electron content variations during the 15 January 2010 and 21 June 2020 solar eclipse", Radio Science **56** (2021) 1. https://doi.org/10.1029/2020RS007215.
[6] S. I. Akasofu, "Energy coupling between the solar wind and the magnetosphere", Space Science Reviews **28** (1981) 121. https://doi.org/10.1007/BF00218810.
[7] W. D. Gonzalez, B. T. Tsurutani & A. L. Clúa de Gonzalez, "Interplanetary origin of geomagnetic storms", Space Science Reviews **88** (1999) 529. https://doi.org/10.1023/A:1005160129098.
[8] C. Wang, J. P. Han, H. Li, Z. Peng & J. D. Richardson, "Solar wind-magnetosphere energy coupling function fitting: Results from a global MHD simulation", Journal of Geophysical Research: Space Physics **119** (2014) 6199. https://doi.org/10.1002/2014JA019834.
[9] V. H. Luu, *Etude du champ électromagnétique et interprétation de données magnétotellurique*, Ph.D. dissertation, Département des Sciences de la Terre, Université Paris-Sud, Orsay, France, 2011. https://theses.hal.science/tel-00669815.
[10] M. Sugiura, "Hourly values of equatorial Dst for the IGY", Annals of the International Geophysical Year **35** (1964) 9. Available online: https://ntrs.nasa.gov/api/citations/19650020355/downloads/19650020355.pdf.
[11] G. Rostoker, "Geomagnetic indices", Reviews of Geophysics **10** (1972) 935. https://doi.org/10.1029/RG010i004p00935.
[12] H. Lundstedt, H. Gleisner & P. Wintoft, "Operational forecasts of the geomagnetic Dst index", Geophysical Research Letters **29** (2002) 34. https://doi.org/10.1029/2002GL016151.

[13] N. Yu. Ganushkina, M. W. Liemohn & S. Dubyagin, "Current Systems in the Earth's Magnetosphere", Reviews of Geophysics **56** (2018) 309. https://doi.org/10.1002/2017RG000590.

[14] T. N. Davis & M. Sugiura, "Auroral electrojet activity index AE and its universal time variations", Journal of Geophysical Research **71** (1966) 785. https://doi.org/10.1029/JZ071i003p00785.

[15] R. M. Katus & M. W. Liemohn, "Similarities and differences in low-to middle-latitude geomagnetic indices", Journal of Geophysical Research: Space Physics **118** (2013) 5149. https://doi.org/10.1002/jgra.50510.

[16] R. Hajra, B. T. Tsurutani & G. S. Lakhina, "The complex space weather events of 2017 September", The Astrophysical Journal **899** (2020) 3. https://doi.org/10.3847/1538-4357/ab9c79.

[17] B. T. Tsurutani & R. Hajra, "The interplanetary and magnetospheric causes of geomagnetically induced currents (GICs) > 10 A in the Mäntsälä Finland pipeline: 1999 through 2019", Journal of Space Weather and Space Climate **11** (2021) 23. https://doi.org/10.1051/swsc/2021032.

[18] R. K. Burton, R. L. McPherron & C. T. Russell, "An empirical relationship between interplanetary conditions and Dst", Journal of Geophysical Research **80** (1975) 4204. https://doi.org/10.1029/JA080i031p04204.

[19] G. S. Lakhina & B. T. Tsurutani, "Geomagnetic storms: Historical perspective to modern view", Geoscience Letters **3** (2016) 1. https://doi.org/10.1186/s40562-016-0037-4.

[20] P. Riley & J. J. Love, "Extreme geomagnetic storms: Probabilistic forecasts and their uncertainties", Space weather **15** (2017) 53.https://doi.org/10.1002/2016SW001470.

[21] E. Camporeale, "The challenge of machine learning in space weather: Nowcasting and forecasting", Space weather **17** (2019) 1166. https://doi.org/10.1029/2018SW002061.

[22] D. Sierra-Porta, J. D. Petro-Ramos, D. J. Ruiz-Morales, D. D. Herrera-Acevedo, A. F. García-Teheran & M. T. Alvarado, "Machine learning models for predicting geomagnetic storms across five solar cycles using Dst index and heliospheric variables", Advances in Space Research **74** (2024) 3483. https://doi.org/10.1016/j.asr.2024.04.014.

[23] Y. Peng, "Advancement and limitations in geomagnetic storm prediction models", 3rd International Conference on Environmental Geoscience and Earth Ecology, Auckland, New Zealand, 2025, pp. 52–58. https://doi.org/10.54254/2753-8818/81/2025.21052

[24] W. D. Gonzalez, J. A. Joselyn, Y. Kamide, H. W. Kroehl, G. Rostoker, B. T. Tsurutani & V. M. Vasyliunas, "What is a geomagnetic storm?" Journal of Geophysical Research: Space Physics **99** (1994) 5771. https://doi.org/10.1029/94JA00470.

[25] C. A. Loewe & G. W. Prölss, "Classification and mean behavior of magnetic storms", Journal of Geophysical Research: Space Physics **102** (1997) 14209. https://doi.org/10.1029/96JA04020.

[26] J. T. Gosling, D. J. McComas, J. L. Phillips & S. J. Bame, "Geomagnetic activity associated with earth passage of interplanetary shock disturbances and coronal mass ejections", Journal of Geophysical Research: Space Research **96** (1991) 7831. https://doi.org/10.1029/91JA00316.

[27] D. F. Webb, E. W. Cliver, N. U. Crooker, O. C. St. Cyr & B. J. Thompson, "Relationship of halo coronal mass ejections, magnetic clouds, and magnetic storms", Journal of Geophysical Research: Space Physics **105** (2000) 7491. https://doi.org/10.1029/1999JA000275.

[28] K. E. J. Huttunen, R. Schwenn, V. Bothmer & H. E. J. Koskinen, "Properties and geoeffectiveness of magnetic clouds in the rising, maximum and early declining phases of solar cycle 23", Annales Geophysicae **23** (2005) 625. https://doi.org/10.5194/angeo-23-625-2005.

[29] I. G. Richardson & H. V. Cane, "Solar wind drivers of geomagnetic storms during more than four solar cycles", Journal of Space Weather and Space Climate **2** (2012) A01. https://doi.org/10.1051/swsc/2012001.

[30] E. K. J. Kilpua, J. G. Luhmann, L. K. Jian, C. T. Russell & Y. Li, "Why have geomagnetic storms been so weak during the recent solar minimum and the rising phase of cycle 24?" Journal of Atmospheric and Solar-Terrestrial Physics **107** (2014) 12. https://doi.org/10.1016/j.jastp.2013.11.001.

[31] W. I. Axford, "Magnetospheric convection", Reviews of Geophysics **7** (1969) 421. https://doi.org/10.1029/RG007i001p00421.

[32] V. M. Vasyliunas, "Mathematical models of magnetospheric convection and its coupling to the ionosphere", in *Particles and Fields in the Magnetosphere*, B. M. McCormac (Ed.), Springer, Dordrecht, Netherlands, 1970, pp. 60–71. https://doi.org/10.1007/978-94-010-3284-1_6.

[33] C. R. Chappell, "Detached plasma regions in the magnetosphere", Journal of Geophysical Research **79** (1974) 1861. https://doi.org/10.1029/JA079i013p01861.

[34] J. W. Dungey, "Interplanetary magnetic field and the auroral zones", Physical Review Letters **6** (1961) 47. https://doi.org/10.1103/PhysRevLett.6.47.

[35] J. W. Dungey, "Interactions of solar plasma with the geomagnetic field", Planetary and Space Science **10** (1963) 233. https://doi.org/10.1016/0032-0633(63)90020-6.

[36] D. L. Carpenter, "Relations between the dawn minimum in the equatorial radius of the plasmapause and Dst, Kp, and local K at Byrd Station", Journal of Geophysical Research **72** (1967) 2969. https://doi.org/10.1029/JZ072i011p02969.

[37] M. J. Rycroft & J. O. Thomas, "The magnetospheric plasmapause and the electron density trough at the Alouette I orbit", Planetary and Space Science **18** (1970) 65. https://doi.org/10.1016/0032-0633(70)90067-X.

[38] W. Lei, R. Gendrin, B. Higel & J. Berchem, "Relationships between the solar wind electric field and the magnetospheric convection electric field", Geophysical Research Letters **8** (1981) 1099. https://doi.org/10.1029/GL008i010p01099.

[39] V. Bothmer & I. A. Daglis, *Space Weather—Physics and Effects*, Springer, Berlin and Heidelberg, Germany, 2007, pp. 103–130. https://doi.org/10.1007/978-3-540-34578-7_4.

[40] K. Salfo & O. Frédéric, "Magnetosphere convection electric field (MCEF) time variation from 1964 to 2009: Investigation on the signatures of the geoeffectiveness coronal mass ejections", International Journal of Physical Sciences **13** (2018) 273. https://doi.org/10.5897/IJPS2018.4759.

[41] I. Kacem, C. Jacquey, V. Génot, B. Lavraud, Y. Vernisse, A. Marchaudon, O. Le Contel, H. Breuillard, T. D. Phan, H. Hasegawa & M. Oka, "Magnetic reconnection at a thin current sheet separating two interlaced flux tubes at the Earth's magnetopause", Journal of Geophysical Research: Space Physics **123** (2018) 1779. https://doi.org/10.1002/2017JA024537.

[42] A. Marchaudon, *Observation et modélisation des processus de couplage entre la magnétosphère et l'ionosphère terrestres*, Ph.D. dissertation, Laboratoire d'Aérologie, Université Paul Sabatier, Toulouse, France, 2018. https://hal.science/tel-01959258v1.

[43] I. Revah & P. Bauer, *Rapport d'activité du Centre de Recherches en Physique de l'environnement Terrestre et Planétaire*, CRPE, Issy-les-Moulineaux, France, 1982, pp. 38–40. https://hal-lara.archives-ouvertes.fr/hal-02192225.

[44] D. F. Smart, H. B. Garrett & M. A. Shea, "The prediction of AE, Ap, and Dst at time lags between 0 and 30 hours", Solar Terrestrial Prediction Proceedings, Boulder, Colorado, USA, 1979, pp. 399–414. https://ntrs.nasa.gov/citations/19800016214.

[45] D. N. Baker, E. W. Hones Jr, J. B. Payne & W. C. Feldman, "A high time resolution study of interplanetary parameter correlations with AE", Geophysical Research Letters **8** (1981) 179. https://doi.org/10.1029/GL008i002p00179.

[46] A. Meloni, A. Wolfe & L. J. Lanzerotti, "On the relationships between interplanetary quantities and the global auroral electrojet index", Journal of Geophysical Research: Space Physics **87** (1982) 119. https://doi.org/10.1029/JA087iA01p00119.

[47] Y. Nishimura, T. Kikuchi, J. Wygant, A. Shinbori, T. Ono, A. Matsuoka, T. Nagatsuma & D. Brautigam, "Response of convection electric fields in the magnetosphere to IMF orientation change", Journal of Geophysical Research: Space Physics **114** (2009) A09206. https://doi.org/10.1029/2009JA014277.

[48] G. Rostoker, H.-L. Lam, & W. D. Hume,"Response time of the magnetosphere to the interplanetary electric field", Canadian Journal of Physics **50** (1972) 544. https://doi.org/10.1139/p72-073.

[49] G. Inza, Z. Christian, K. Salfo & O. Frédéric, "Variability of the magnetospheric electric field due to high-speed solar wind convection from 1964 to 2009", African Journal of Environmental Science and Technology **16** (2022) 1. https://doi.org/10.5897/AJEST2021.3075.

[50] G. Inza, G. Karim, & O. Frédéric, "Magnetospheric Convective Electric Field (MCEF): Comparative Diurnal Statistical Variability of Different Types of Shock and Magnetic Cloud Activity Days", International Journal of Geosciences **16** (2025) 189. https://doi.org/10.4236/ijg.2025.164010.

[51] K. Salfo, G. A. M. Frédéric, G. Inza & O. Frédéric, "Diurnal variability of the magnetospheric convective electric field (MCEF) from 1996 to 2019: Comparative investigation into the signatures of the geoeffective-

ness of coronal mass ejections and magnetic clouds", Scientific Research and Essays **18** (2023) 45. https://doi.org/10.5897/SRE2023.6772.

[52] D. A. Stéphane, K. Salfo, S. S. Alphonse & O. Frédéric, "Variability of the electric field of magnetospheric convection in recurrent activity during the solar cycle 24", International Journal of Physical Sciences 1**8** (2023) 129. https://doi.org/10.5987/IJPS2023.5039.

[53] N. Bazié, C. Zoundi, A. J. S. Dama & F. Ouattara, "Variability of the Magnetospheric Convection Electric Field (MCEF) Under Shock Activity During the Solar Cycle 24", Applied Physics Research **16** (2024) 134. https://doi.org/10.5539/apr.v16n1p134.

[54] J. Legrand & P. Simon, "Solar cycle and geomagnetic activity: A review for geophysicists. Part I. The contributions to geomagnetic activity", Annales geophysicae **7** (1989) 565. Available online: https://www.ipgp.fr/~legoff/Download-PDF/Soleil-Climat/IndicesAA/annales-geophysicaeI-89-7-565-578.pdf.

[55] J. L. Zerbo, C. Amory Mazaudier, F. Ouattara & J. D. Richardson, "Solar wind and geomagnetism: toward a standard classification of geomagnetic activity from 1868 to 2009", Annales Geophysicae **30** (2012) 421. https://doi.org/10.5194/angeo-30-421-2012.

[56] I. Azzouzi, *Impact des événements solaires sur l'ionisation de l'ionosphére des moyennes et basses latitudes dans le secteur Europe-Afrique*, Ph.D. dissertation, Département de Physique, Université Pierre et Marie Curie - Paris VI and Université Mohammed V, Rabat, Morocco, 2016. https://theses.hal.science/tel-01883930.

[57] B. Nongobsom, K. Salfo, G. Karim & O. Frédéric, "Response of the Magnetospheric Convection Electric Field (MCEF) to Geomagnetic Storms During the Solar Cycle 24 Maximum Phase", International Journal of Geophysics **2025** (2025) 9888419. https://doi.org/10.1155/ijge/9888419.

[58] M. C. Kelley, B. G. Fejer & C. A. Gonzales, "An explanation for anomalous equatorial ionospheric electric fields associated with a northward turning of the interplanetary magnetic field", Geophysical Research Letters **6** (1979) 301. https://doi.org/10.1029/GL006i004p00301.

[59] A. Singh, V. S. Rathore, R. P. Singh & A. K. Singh, "Source identification of moderate ($-100$ nT $<$ Dst $<$ $-50$ nT) and intense geomagnetic storms (Dst $<$ $-100$ nT) during ascending phase of solar cycle 24", Advances in Space Research, **59** (2017), 1209. https://doi.org/10.1016/j.asr.2016.12.006.

[60] P. M. de Siqueira, E. R. de Paula, M. Muella, L. F. C. Rezende, M. A. Abdu & W. D. Gonzalez, "Storm-time total electron content and its response to penetration electric fields over South America", Annales Geophysicae **29** (2011) 1765. https://doi.org/10.5194/angeo-29-1765-2011.

[61] S. V. Badman & S. W. H. Cowley, "Significance of Dungey-cycle flows in Jupiter's and Saturn's magnetospheres, and their identification on closed equatorial field lines", Annales Geophysicae **25** (2007) 941. https://doi.org/10.5194/angeo-25-941-2007.

[62] G. L. Siscoe, C. J. Farrugia & P. E. Sandholt, "Comparison between the two basic modes of magnetospheric convection: convection modes compared", Journal of Geophysical Research **116** (2011) A5201. https://doi.org/10.1029/2010JA015842.

[63] A. Singh, V. S. Rathore, S. Kumar, S. S. Rao, S. K. Singh & A. K. Singh, "Effect of intense geomagnetic storms on low-latitude TEC during the ascending phase of the solar cycle 24", Journal of Astrophysics and Astronomy **42** (2021) 99. https://doi.org/10.1007/s12036-021-09774-8.

[64] L. P. Shadrina, "Two types of geomagnetic storms and relationship between Dst and AE indexes", E3S Web of Conferences **20** (2017) 01010. https://doi.org/10.1051/e3sconf/20172001010.